

Molecular Arrangement and Charge Transfer in C₆₀/Graphene Heterostructures

Claudia Ojeda-Aristizabal,^{*,†,‡,§,⊗,○} Elton J. G. Santos,^{*,||,&,∇,○} Seita Onishi,^{†,‡,§} Aiming Yan,^{†,‡,§} Haider I. Rasool,^{†,‡,§} Salman Kahn,[†] Yinchuan Lv,[†] Drew W. Latzke,^{‡,§} Jairo Velasco, Jr.,[†] Michael F. Crommie,^{†,‡,§} Matthew Sorensen,[†] Kenneth Gotlieb,^{‡,§} Chiu-Yun Lin,[‡] Kenji Watanabe,^{⊥,○} Takashi Taniguchi,[⊥] Alessandra Lanzara,^{†,‡} and Alex Zettl^{*,†,‡,§}

[†]Department of Physics, University of California, Berkeley, California 94720, United States

[‡]Materials Sciences Division, Lawrence Berkeley National Laboratory, Berkeley, California 94720, United States

[§]Graduate Group in Applied Science and Technology, University of California, Berkeley, California 94720, United States

^{||}Department of Chemical Engineering, Stanford University, Stanford, California 94305, United States

[⊥]Advanced Materials Laboratory, National Institute for Materials Science, 1-1 Namiki Tsukuba, Ibaraki 305-0044, Japan

[⊗]Kavli Energy NanoSciences Institute at the University of California, Berkeley and the Lawrence Berkeley National Laboratory, Berkeley, California 94720, United States

[⊙]Department of Physics & Astronomy, California State University Long Beach, Long Beach, California 90840, United States

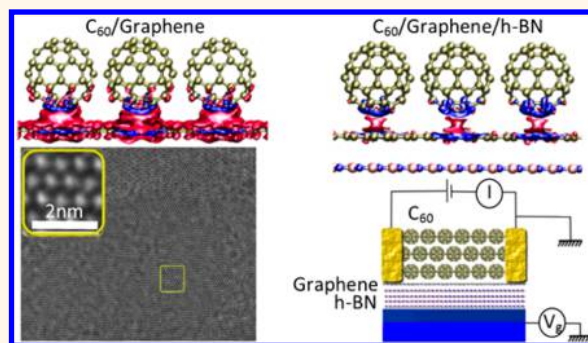
[&]School of Mathematics and Physics, Queen's University Belfast, Belfast BT7 1NN, United Kingdom

[∇]School of Chemistry and Chemical Engineering, Queen's University Belfast, Belfast BT7 1NN, United Kingdom

S Supporting Information

ABSTRACT: Charge transfer at the interface between dissimilar materials is at the heart of electronics and photovoltaics. Here we study the molecular orientation, electronic structure, and local charge transfer at the interface region of C₆₀ deposited on graphene, with and without supporting substrates such as hexagonal boron nitride. We employ *ab initio* density functional theory with van der Waals interactions and experimentally characterize interface devices using high-resolution transmission electron microscopy and electronic transport. Charge transfer between C₆₀ and the graphene is found to be sensitive to the nature of the underlying supporting substrate and to the crystallinity and local orientation of the C₆₀. Even at room temperature, C₆₀ molecules interfaced to graphene are orientationally locked into position. High electron and hole mobilities are preserved in graphene with crystalline C₆₀ overlayers, which has ramifications for organic high-mobility field-effect devices.

KEYWORDS: graphene, C₆₀, organic semiconducting molecules, fullerenes, interfacial charge transfer



C₆₀ and graphene are, in their own right, fascinating low-dimensional materials with spectacular properties. The high electron affinity and unusual phonon modes of C₆₀ have rendered it an important nanomaterial for electronic applications, and the ultrafast charge transfer dynamics and an energetically favorable LUMO level for many donor organic semiconductors have established C₆₀ as an excellent electron acceptor for organic solar cells.^{1,2} When combined with strong charge transfer from alkali metals, the phonon modes in C₆₀ drive superconductivity at surprisingly high temperature.³ The related carbon allotrope graphene displays phenomenal electron and hole mobilities even at room temperature, and the conductance can be readily gated by an external electric

field or altered via adsorbed chemical species. It is likely that many applications of graphene will involve heterostructures. Indeed, the interfacing of graphene to other low-2D materials via van der Waals forces is a rapidly expanding field of research.^{4,6,19}

The interfacing of C₆₀ and graphene is of particular interest. For example, charge transfer between C₆₀ and graphene affects the graphene electronic transport.^{26–29} Adding gating electric fields^{7,8} allows further functional possibilities on the control of

Received: January 24, 2017

Accepted: April 24, 2017

Published: April 24, 2017

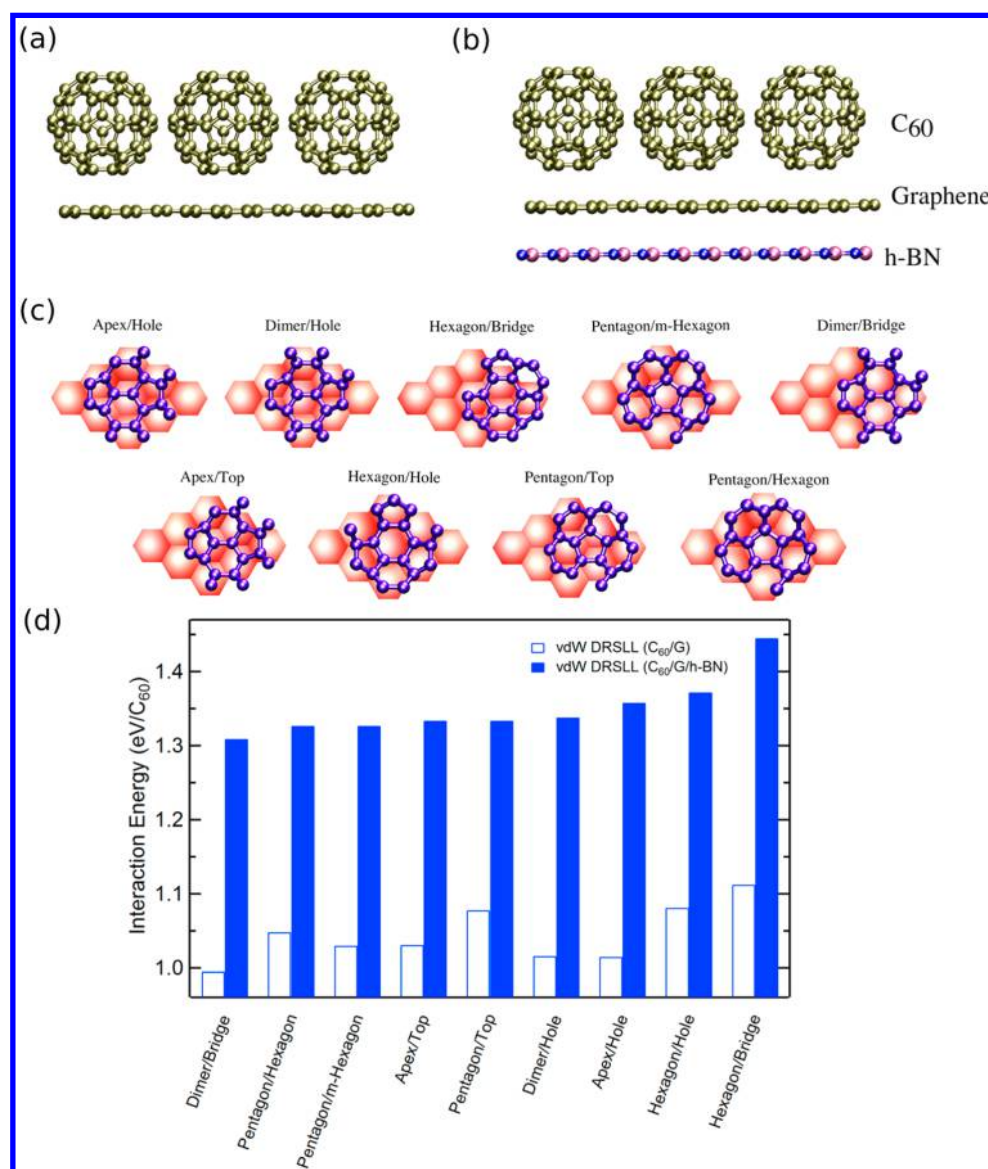


Figure 1. Schematic representation of (a) C₆₀ molecules on graphene (C₆₀/G) and (b) C₆₀ molecules on graphene supported by h-BN (C₆₀/G/h-BN). The relative separation between C₆₀, graphene, and h-BN has been initially converged. (c) Optimized molecular configurations between C₆₀ and graphene resulting from a computational screening at different starting geometries. For clarity, C₆₀ molecules (violet atoms) are only shown near the graphene surface (faint pink) with the rest of the other atoms hidden. (d) Interaction energies per C₆₀ molecule calculated with vdW interactions included for the different configurations shown in (c). The interaction energy is defined in terms of the adsorption energies between C₆₀ and G or the G/h-BN heterostructure: $E_i = E[C_{60}] + E[A] - E[C_{60}/A]$, where A = G, G/h-BN. The open bars are for C₆₀/G, while the solid blue bars are for C₆₀/G/h-BN.

interface properties such as energy barriers, magnetism,^{9,10} and electron–hole dynamics.^{4,11} The ability to fine-tune the charge transfer state of C₆₀ interfaced to graphene (e.g., with reversible electrostatic gating) is thus central to the development of novel electrochemical and optoelectronic prototypes. Devices based on organic molecule/graphene interfaces, which utilize the tunable Fermi level in graphene, have already shown promise.^{12–14} In particular, the C₆₀/graphene heterostructure is known to form a Schottky junction.¹³

In this report, we investigate the C₆₀/graphene interface *via ab initio* density functional theory (DFT) calculations, transmission electron microscopy, and electronic transport experiments at cryogenic temperature and at room temperature. The graphene is either suspended or supported on different substrates, including hexagonal boron nitride (h-BN).

We determine the most favorable molecular orientations of the C₆₀'s, the interface band structure, the intrinsic charge transfer (which is highly dependent on C₆₀ deposition process and substrate type), and the graphene electron and hole mobilities. The theoretical and experimental evidence suggests that C₆₀ molecules at the interface remain firmly locked to the graphene lattice even at room temperature, in sharp contrast to the freely rotating behavior of C₆₀s in undoped molecular crystals.

RESULTS AND DISCUSSION

We first examine theoretically the most favorable geometrical arrangements of crystalline close-packed C₆₀ on graphene on different substrates at low temperatures and the associated interfacial band structure and charge transfer. Parts a and b of Figure 1 show schematic representations respectively of C₆₀ on

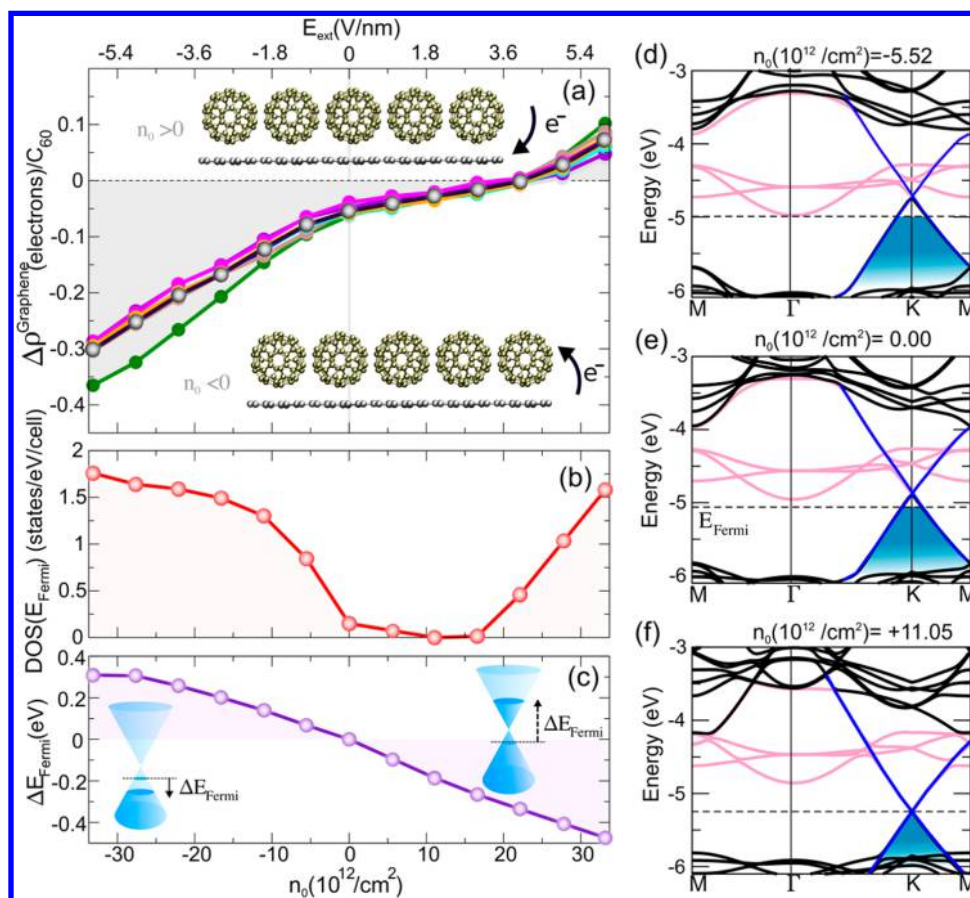


Figure 2. First-principles density functional theory calculations for C₆₀/graphene (C₆₀/G) interfaces. (a) Calculated charge transfer (in electrons per C₆₀ interfacial molecule) to graphene as a function of the external electric field (E_{ext}) induced-carrier density in graphene (n_0). Both scales are represented along the x -axis. All nine C₆₀/graphene geometries presented in Figure 1c are represented, with several data curves superimposed on top of each other at the present density scale. The black curve shows the average of all configurations. The green curve (dimer/hole) has a slightly larger charge transfer at large values of n_0 . A cut through the data set at $n_0 = 0$, with the different configurations identified, is presented in Figure 3a. Positive $\Delta\rho$ means that electrons are transferred from C₆₀ to graphene, which can occur with sufficient gate bias (*i.e.*, high enough positive n_0). (b) Variation of the density of states at the Fermi level as a function of n_0 for the dimer/hole configuration of C₆₀/G. Similar results are also observed for the other interface geometries (not shown). (c) Variation of the Fermi level of the combined C₆₀/G system as a function of n_0 . Notice that the position of the Fermi level is relative to that at zero bias where a finite charge transfer is already observed. Positive (negative) bias shifts upward (downward) in energy the Fermi level (insets). (d–f) Electronic band structures of the C₆₀/G heterostructure with a dimer/hole configuration at different gate bias. Graphene states are highlighted in blue and C₆₀ bands in faint red. Fermi level is shown by the dashed line in each panel.

suspended graphene and C₆₀ on graphene supported by h-BN. The C₆₀ film is assumed to be crystalline with a well-ordered periodic lattice, and a 4 × 4 superstructure is defined. In the nomenclature of ref 13, the C₆₀ lattice is oriented 28° with respect to the graphene lattice; *i.e.*, it is aligned with the armchair direction. Due to the highly spherical shape of the C₆₀ molecule, several possible molecular arrangements for C₆₀ on graphene are possible, with different interaction energies and different local charge transfer.

As in ref 13, we consider nine representative orientations of C₆₀ on graphene (Figure 1c). We perform first-principles density functional theory calculations including van der Waals (vdW) dispersion forces (the calculation approach differs somewhat from that of ref 13; see the Methods for details). If vdW interactions are excluded (using the PBE functional approach, see the Methods), then the most energetically favorable configuration of C₆₀ on graphene is the hexagon/hole alignment. However, if vdW interactions are included (using the DRSL functional approach), then, as presented in Figure 1d (open bars), the most energetically favorable configuration

is the hexagon/bridge alignment (right-hand-most open bar), with an interaction energy of about 1.1 eV/C₆₀. We note that the vdW term is significant, with a jump in interaction energy of roughly 1 eV/C₆₀, as shown previously.¹³ If an h-BN support is added to the graphene (see Figure 1b), the interaction energy (including vdW interactions) between graphene and C₆₀ is further enhanced by ~0.25–0.33 eV, as seen by comparing the open and filled bars in Figure 1d. With an h-BN supporting substrate, the most energetically favorable configuration at low temperatures of C₆₀ on graphene remains hexagon/bridge (Figure 1d, right-hand-most filled bar), with an interaction energy of about 1.45 eV/C₆₀.

Different molecular orientations of C₆₀ on graphene give different magnitudes of charge transfer between the C₆₀ and graphene. We use first-principles DFT simulations to evaluate the magnitude and sign of the charge transfer. Even though DFT is known to underestimate band gaps and frontier orbitals (HOMO, LUMO), we will show below that our calculations reproduce closely the magnitudes and trends observed in the experiments for the large systems used in the supercell. The

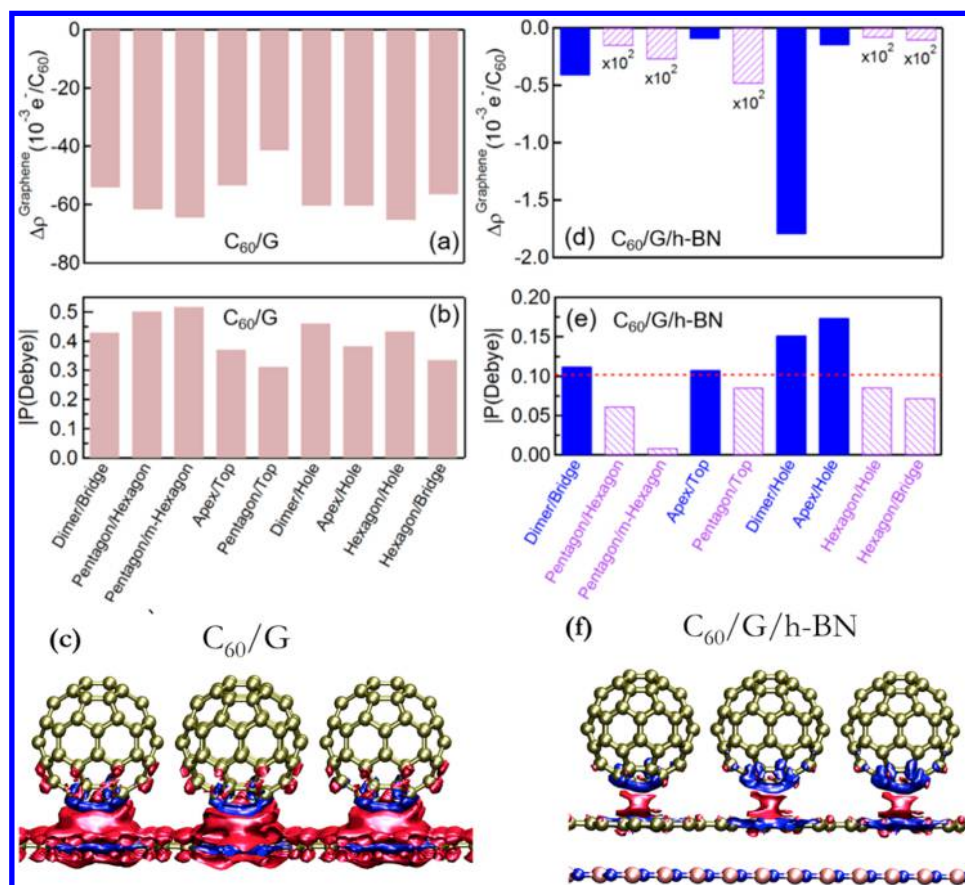


Figure 3. vdW–DFT calculations for total interfacial charge transfer, induced dipole moment, and charge-difference density for the C_{60}/G and $C_{60}/G/h\text{-BN}$ systems, all for $n_0 = 0$. (a) Charge transfer and (b) induced dipole moment for C_{60}/G . The dipole moment vector points from C_{60} to graphene. (c) Charge difference density for C_{60}/G assuming a dimer/hole orientation. (d) Charge transfer and (e) induced dipole moment for $C_{60}/G/h\text{-BN}$. In (d), data for the hatched purple open bars have been amplified by 10^2 for readability. The dashed horizontal red line in (e) delineates an induced dipole threshold of 0.1 D. Dipole data above this are plotted in solid blue, while data below this are plotted in hatched purple (see text). (f) Charge difference density for $C_{60}/G/h\text{-BN}$ assuming a dimer/hole orientation. For (c) and (f), blue and red isosurfaces represent positive and negative charges, respectively.

system size is too large for higher levels of theory, *e.g.*, GW or hybrid functional, to be employed. We consider first the case of C_{60} on suspended graphene. Figure 2a shows the calculated charge transfer from C_{60} to graphene for the different C_{60} orientations, as a function of n_0 , the externally induced graphene charge density (as might result from external electric field gating). With zero external gating ($n_0 = 0$), the charge transfer is negative in the range 0.03–0.07 electrons/ C_{60} (this corresponds to a change in charge density in the graphene of $4.3\text{--}10.1 \times 10^{12}/\text{cm}^2$). For all molecular orientations, with no external gating, C_{60} on suspended graphene acts as an electron acceptor, as expected. With increasing n_0 in the negative direction, the charge transfer between C_{60} and graphene increases, with the dimer/hole orientation giving a slightly bigger effect. With increasing n_0 in the positive direction, external gating compensates the intrinsic charge transfer, with a zero crossing at about $n_0 = +20 \times 10^{12}/\text{cm}^2$. Beyond this, external gating overcomes the intrinsic charge flow and the C_{60} is forced to donate electrons to the graphene.

Parts b and c of Figure 2 show, respectively, the influence of external gating (again expressed as n_0) on the graphene electronic density of states and Fermi level shift for the $C_{60}/$ graphene hybrid system assuming a dimer/hole configuration. Similar results are obtained for the other orientations. The effect of electrostatic gating on the electronic band structure is

displayed in Figure 2d–f, which clearly shows the charge-doping effect at the Dirac point and the rigid shiftlike effect of the electric gating on C_{60} and graphene bands. Once the $C_{60}/$ graphene interface is created, at no bias regime $n_0 = 0$, the HOMO of the C_{60} layer (faint red in Figure 2e) is sufficiently lower in energy relative to the Fermi level, and charge transfer takes place from graphene to C_{60} . At finite bias (Figure 2d,f), the potential difference between graphene and C_{60} drives the position of the fullerene states closer (for $n_0 < 0$) or away (for $n_0 > 0$) from the Fermi level by several tenths of meV's. This particular arrangement of graphene and C_{60} states drives the system to a band alignment where most of the states are bias-dependent, allowing further control on the electronic structure.

Parts a and b of Figure 3 contrast, for $C_{60}/$ graphene with $n_0 = 0$, the charge transfer and induced dipole moment $|P(\text{debye})|$ for the selected C_{60} orientations. The induced dipole moments are all in the range $\sim 0.3\text{--}0.5$ D, with no obvious correlation to the induced charge densities. For C_{60}/G , the charge transfer increases with increasing magnitude of dipole moment, but there is much scatter in the data (see Figure S5a). There appears to be no correlation between the C_{60} adsorption orientation dependence of the dipole moment, charge transfer, and interaction energies. Figure 3c shows the zero bias charge difference density plot for the dimer/hole configuration for the $C_{60}/$ graphene heterostructure.

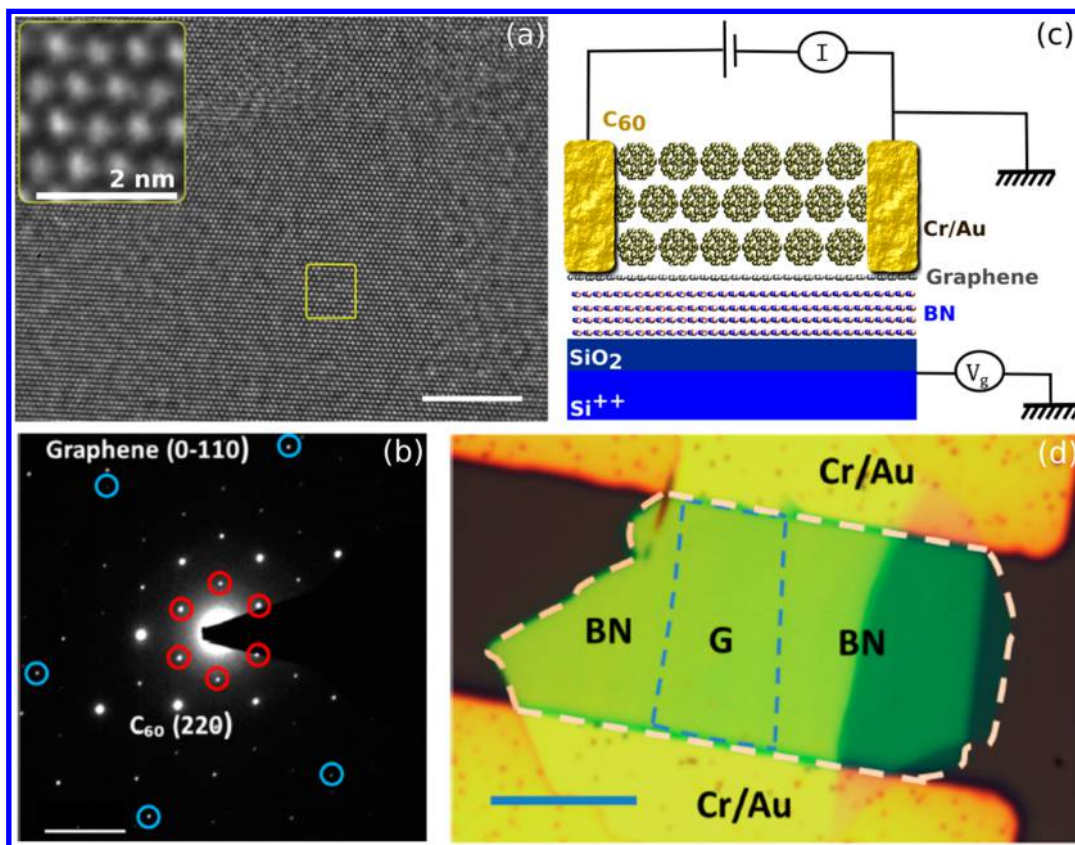


Figure 4. (a) TEM image of a ~ 15 nm thick C_{60} film deposited on suspended graphene under UHV conditions. High crystallinity is clearly observed (scale bar 10 nm). The inset is a blow-up of the region outlined by the yellow box and highlights the close-packed structure of the C_{60} s (bright dots correspond to the projected lattice images of the C_{60} molecular columns). (b) Electron diffraction for C_{60} deposited on suspended graphene under UHV conditions. Graphene (blue circles) and C_{60} (red circles) diffraction spots are identified (scale bar 2 nm^{-1}). (c) Schematic representation of C_{60} /G/h-BN device used for transport measurements. The device can be electrically probed prior to, and after, C_{60} deposition. (d) Optical image of a G/h-BN heterostructure contacted with Cr/Au electrodes prior to C_{60} deposition. The dotted lines indicate the border of the graphene (blue) and h-BN (pink) flakes (scale bar $20 \mu\text{m}$).

We now turn to the additional influence of a supporting h-BN substrate on the charge transfer from C_{60} to graphene. Figure 3d shows the predicted charge transfer from C_{60} to graphene for the different molecular orientations of C_{60} , all for the bias-free condition $n_0 = 0$. In all cases, the charge transfer is negative (electrons again flow from graphene to C_{60}), and the dimer/hole orientation has maximum charge transfer. The orientation with the maximum charge transfer (dimer/hole) is different from the orientation with the strongest interaction energy (hexagon/bridge), which implies that more charge transfer does not necessarily cause stronger molecular interaction. The interaction of C_{60} with the substrate is an interplay between vdW interaction at the C_{60} /graphene interface and charge rearrangement at the graphene/h-BN interface. Hence, it is possible that the vdW interaction is not determined solely by charge transfer. As the spread in interaction energies among the C_{60} molecular orientations is small (0.020–0.100 eV), it is possible to establish more than one C_{60} molecular orientation. Because of this complication, further study is needed to exactly determine the trade-off between the driving forces in this system. Remarkably, the addition of the h-BN substrate reduces the maximum (bias-free) charge transfer by roughly 1 order of magnitude from that of the C_{60} /graphene configuration (Figure 3a). Figure 3e shows the corresponding induced dipole moment $|P(\text{debye})|$. Interestingly, with an h-BN substrate present, the polarizations

for the nine molecular arrangements can be separated into two groups, delineated by a threshold polarization $|P(\text{debye})|_{\text{thresh}} = 0.10$, as indicated by the dotted line in Figure 3e. Results for the group above threshold are displayed with blue bars and give sizable charge transfer in the range of $(0.01\text{--}0.28) \times 10^{12} / \text{cm}^2$ ($(0.07\text{--}2) \times 10^{-3} e/C_{60}$). Results for the group below threshold are displayed in purple and give charge transfers 3 orders of magnitude lower. For C_{60} /G/h-BN, there is no clear correlation between charge transfer and dipole moment (see Figure S5b). The only notable qualitative trend is that the group of molecular orientations with large dipole moments corresponds to the group with large charge transfer, and the same goes for the group of small dipole moments and charge transfer. The greatest charge transfer is obtained from the dimer/hole configuration ($1.8 \times 10^{-3} e/C_{60}$). The charge transfer varies significantly across the C_{60} configurations due to the importance of the carbon bond between two hexagons of the C_{60} cage, namely 6:6. According to the chemistry of C_{60} ,^{16,17} 6:6 bonds are preferential sites for functionalization for several compounds as the degree of electron delocalization varies (double bond) and higher reactivity is present, mainly due to the increase of π electron density at this bond.

Although h-BN is often considered to be an ideal, inert substrate for graphene,¹⁸ our results clearly show that it has a profound effect on heterostructure charge transfer and polarizability. Figure 3f presents the charge difference density

plot at zero bias for the dimer/hole configuration for C_{60} /graphene/h-BN. The stronger charge transfer for C_{60} on the suspended graphene with no underlying h-BN (Figure 3c) is strikingly evident. Prior to forming the interface with C_{60} , the induced dipole moment at the graphene/h-BN heterostructure is $|P(\text{debye})| \approx 0.33$ (see Figure S4). After formation of the interface with C_{60} , charge rearrangement takes place and the value reduces to below $|P(\text{debye})| \approx 0.10$. The difference in electronic character for the p_z -orbitals between h-BN, polar, and graphene, covalent, is one of the main driving forces for such modifications of the interfacial polarization dipole. No appreciable modifications ($<0.10 \text{ \AA}$) of the value of the interlayer distance between graphene and C_{60} are observed due to this charge rearrangement once monolayer or few-layer h-BN are introduced. This suggests the active electronic role of the h-BN substrate in limiting the amount of carriers that participates in the interfacial charge separation.

We note that the theoretical studies described above are performed in the low temperature ($T = 0$) regime. The question arises what influence higher temperature might have on the results. For example, it is well-known that in (undoped) crystalline C_{60} the C_{60} molecules freely rotate at room temperature.^{1,2} Near 260 K, the C_{60} 's rotate almost freely, and in the range 260–90 K they execute jumps. Below 90 K, the C_{60} 's are substantially frozen in place.¹ On the other hand, for alkali-doped C_{60} , the situation is quite different. Here, the C_{60} 's are locked into specific orientations with respect to the alkali ions, even at room temperature. X-ray diffraction studies on K_3C_{60} clearly find the absence of C_{60} free rotations.³ For K_3C_{60} and Rb_3C_{60} , the C_{60} s orient themselves so that the electron-rich C=C bonds face the K^+ and Rb^+ ions for charge transfer. Combined with effects of molecular repulsion, C_{60} molecules are fixed to one of the two energetically stable orientations and switch between the two with thermal energy.^{1,2} For ions with smaller ionic radii, such as Li^+ and Na^+ , the ion- C_{60} repulsion is much weaker, but the C_{60} s are still locked to a few energetically stable orientations and jump between them with thermal energy.^{1,2,5}

We have examined theoretically the situation for C_{60} on graphene where the pure C_{60} becomes “doped” (*i.e.*, charged) by virtue of interaction with the (possibly gated) graphene. In this case, the C_{60} 's that reside at the interface with graphene are substantially locked into position even at room temperature as demonstrated using *ab initio* molecular dynamics simulations at 300 K (see the SI and movies for details). Hence, the charge-transfer and band-structure calculations presented above are relevant also for finite temperature. Theoretical simulations predict no temperature dependence of charge transfer up to 300 K.

We now turn to experiment. We explore the following heterostructure: multilayer crystalline C_{60} on monolayer graphene on multilayer h-BN. Figure 4c shows schematically a cross-section of our typical device-like structure, here assuming crystalline C_{60} and an h-BN support. Figure 4d shows an optical image of a functioning device.

We have found that the crystallinity of the C_{60} , and the associated device electronic characteristics, are highly sensitive to C_{60} deposition conditions. If the C_{60} is evaporation-deposited under only modest (1×10^{-4} Torr) “uncontrolled” vacuum conditions, an amorphous C_{60} film typically results (see Figure S1). On the other hand, if the C_{60} deposition is performed under more controlled UHV conditions, highly crystalline C_{60} films are readily obtained. Parts a and b of Figure

4 exemplify the high degree of C_{60} crystallinity of our UHV-prepared samples. For these TEM-compatible samples, 15 nm of C_{60} is deposited on suspended graphene at 1.4×10^{-10} Torr. Excellent crystallinity is observed with a grain size ranging from ~ 100 nm to 200 nm, where the projected lattice images of the stacked layers of C_{60} indicate a triangular pattern for the organization of the molecules (inset in Figure 4a). The crystalline structure is confirmed with electron diffraction as shown in Figure 4b. The outermost spots (blue circles) correspond to the Bragg reflections for the lattice plane (0–110) of graphene (with 2.1 Å spacing).¹⁵ The inner spots (red circles) correspond to Bragg reflections for the lattice plane (111) of C_{60} (with 8.73 Å spacing), which correspond to a close-packed plane with a 2D triangular lattice. This result is consistent with previous results for C_{60} thin films.¹³ Substrate heating is crucial for achieving highly crystalline C_{60} films¹³ (see the Methods).

A controlled deposition of the crystalline C_{60} thin film is essential for quantifying the charge transfer between graphene and C_{60} (see Figure S1). Parts a and b of Figure 5 show R vs V_g

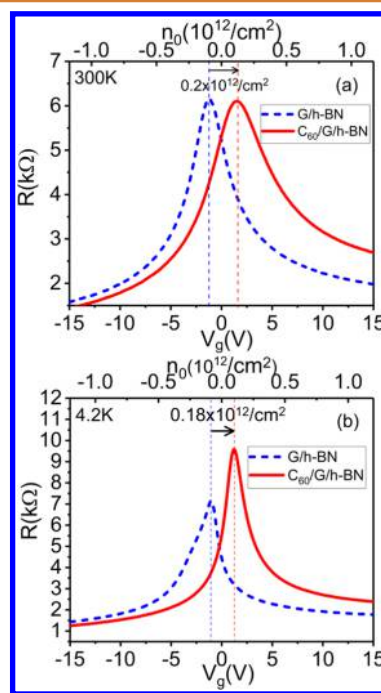


Figure 5. Gate voltage dependence of the resistance of graphene/h-BN devices before (dotted line, blue) and after (solid line, red) deposition of ~ 15 nm high crystallinity C_{60} . Deposition conditions are identical to samples in Figure 4. Samples are measured at (a) 300 K and (b) 4.2 K. Shift of peak to the right indicates hole doping of the graphene by the C_{60} . Mobilities extracted from gate voltage dependence and presented in Table 1.

data for high-quality crystalline C_{60} /graphene/h-BN heterostructures constructed under UHV conditions (1.4×10^{-10} Torr), with a C_{60} thickness of order 50 nm. C_{60} here behaves as an electron acceptor. The room-temperature data of Figure 5a indicate a charge transfer from graphene to C_{60} of $0.2 \times 10^{12}/\text{cm}^2$ or $\Delta\rho = 0.14 \times 10^{-2} e/C_{60}$ transferred from graphene to C_{60} . Figure 5b shows similar data for the same device, but for $T = 4.2$ K. The charge transfer is again $0.2 \times 10^{12}/\text{cm}^2$ or $\Delta\rho = 0.14 \times 10^{-2} e/C_{60}$, in agreement with $\Delta\rho$ theoretically calculated for the dimer/hole C_{60} orientation for a C_{60} /graphene/h-BN heterostructure (see Figure 3d). As predicted

Table 1. Parameters from Electronic-Transport Measurements for a C₆₀/G/h-BN Device^a

T (K)	before C ₆₀ deposition			after C ₆₀ deposition		
	μ_h (cm ² /(V s))	μ_e (cm ² /(V s))	peak position (cm ⁻²)	μ_h (cm ² /(V s))	μ_e (cm ² /(V s))	peak position (cm ⁻²)
4.2	12300	5100	-0.086 ± 0.002	6150	10200	0.095 ± 0.002
300	4700	5830	-0.095 ± 0.003	2530	4600	0.121 ± 0.003

^aHole mobility (μ_h), electron mobility (μ_e) and the gate induced carrier density at which the resistance peaks ("Peak position") are listed for graphene/h-BN before and after C₆₀ deposition.

by molecular dynamics simulations, the absence of temperature dependence results in experimental observation of very close charge transfer values at 4.2 and 300 K.

The carrier mobility is derived from the resistance plots of Figure 5a,b. Knowing the aspect ratio of the sample, the measured resistivity is converted to conductivity and using the Drude model ($\sigma = ne\mu$), and the mobility of the sample is deduced.³⁰ Simple inspection of the slope of the resistance near the charge neutrality point (Figures 5a,b) indicates that the high electron and hole mobilities of graphene in the graphene/h-BN devices are largely preserved after C₆₀ deposition. Table 1 shows that both electron and hole mobilities remain within a factor of 2 after C₆₀ deposition. The room-temperature ($T = 300$ K) data suggest that both the electron and hole mobilities are slightly depressed upon C₆₀ deposition, while the 4.2 K data suggest a depression in the hole mobility, and an increase in the electron mobility, upon C₆₀ deposition. The increase in electron mobility upon C₆₀ deposition is surprising and points to a possible modest annealing effect on the graphene during the (elevated temperature) C₆₀ deposition.

CONCLUSION

In summary, C₆₀/graphene constitutes a van der Waals heterostructure with exciting possibilities for electronic devices and charge-transfer applications. We have shown through first-principles calculations that charge transfer between C₆₀ and graphene depends on C₆₀ orientation and, critically, on the presence or absence of an underlying h-BN substrate. The C₆₀ orientation with the strongest interaction energy is hexagonal/bridge, but the orientation with the greatest charge transfer and dipole moment is dimer/hole. C₆₀'s at the graphene interface are orientationally locked into position and do not rotate, even at room temperature. External gating can change the C₆₀ from an electron acceptor to an electron donor. Crystalline C₆₀/graphene/h-BN devices maintain the high mobility intrinsic to suspended graphene and have a charge transfer consistent with the dimer/hole C₆₀ configuration. Our findings suggest that the combination of *ab initio* density functional theory calculations and electronic transport experiments can be effective in the search for other substrates that enhance the range of tunable charge transfer at the C₆₀/graphene interface.

METHODS

Fabrication of the hBN/Graphene/C₆₀ Heterostructure and Electronic-Transport Measurements. Graphene was mechanically exfoliated from natural graphite on methyl methacrylate polymer. Single graphene flakes were selected and transferred on h-BN, which was previously deposited by mechanical exfoliation on a Si/SiO₂ wafer. Transfer was done following the procedure described in ref 19. Metallic electrodes were deposited using a silicon shadow mask,²⁰ avoiding the use of e-beam resist and further contamination of the surface. After the deposition of the electrodes, the sample was annealed in a H₂/Ar atmosphere at 350 °C for 3 h in order to clean the surface from any organic contamination. Finally, C₆₀ was deposited in ultrahigh vacuum ($P = 1.4 \times 10^{-10}$ Torr) using a low-temperature

effusion cell. The sample was slowly heated from room temperature to 156 °C at a rate of 0.5 K/min. This slow rate protects the integrity of the electrical contact to graphene. Deposition of C₆₀ was done at 0.1 Å/s, heating the effusion cell at 332 °C and holding the sample temperature at 156 °C during deposition. Measurements were performed in a vacuum probe station before and after the deposition of C₆₀ at $P = 1 \times 10^{-8}$ Torr at 300 K and at a lower vacuum at 4.2 K. Two terminal differential resistance measurements were done with a lock-in amplifier applying a small AC current of 10 nA. The carrier density was controlled by applying a DC voltage to the doped silicon.

vdW *ab Initio* Calculations. Calculations were based on *ab initio* density functional theory using the SIESTA method²¹ and the VASP code.^{22,23} Results presented in this work were produced using the VASP code, while SIESTA was used to perform initial tests at large number of atoms in the unit cell. The generalized gradient approximation²⁴ along with the DRSSL²⁵ functional, which includes vdW dispersion forces, were used in both methods, together with a double-polarized basis set in SIESTA and a well-converged plane-wave cutoff of 500 eV in VASP. We used a Fermi–Dirac distribution with an electronic temperature of $k_B T = 20$ meV. Additional details are provided in the Supporting Information.

ASSOCIATED CONTENT

Supporting Information

The Supporting Information is available free of charge on the ACS Publications website at DOI: 10.1021/acsnano.7b00551.

Experimental procedures, Figures S1–S5 (PDF)

Movie showing the dimer/hole configuration (MPG)

Movie showing the dimer/bridge configuration (MPG)

Movie showing the apex/hole configuration (MPG)

AUTHOR INFORMATION

Corresponding Authors

*E-mail: Claudia.Ojeda-Aristizabal@csulb.edu.

*E-mail: e.santos@qub.ac.uk.

*E-mail: azettl@berkeley.edu.

ORCID

Claudia Ojeda-Aristizabal: 0000-0003-0816-9727

Kenji Watanabe: 0000-0003-3701-8119

Author Contributions

○C.O.-A. and E.J.G.S. contributed equally to this work.

Notes

The authors declare no competing financial interest.

ACKNOWLEDGMENTS

C.O.-A. thanks L. Ju for help with sample fabrication and fruitful discussions and K. Kim for advice on C₆₀ deposition. This work was supported in part by the Director, Office of Science, Basic Energy Sciences, Materials Sciences and Engineering Division of the U.S. Department of Energy, under Contract No. DE-AC02-05CH11231 within the sp2-Bonded Materials Program (KC2207), which provided for sample preparation, and within the Molecular Foundry, which provided for TEM characterization, and the National Science

Foundation under Grant No. DMR-1206512, which provided for transport measurements. E.J.G.S. acknowledges the use of computational resources from the UK National High Performance Computing Service, ARCHER, for which access was obtained via the UKCP consortium and funded by EPSRC Grant Ref EP/K013564/1, and the Extreme Science and Engineering Discovery Environment (XSEDE), supported by NSF Grant Nos. TG-DMR120049 and TG-DMR150017. The Queen's Fellow Award through Startup Grant No. M8407MPH and the Energy Sustainable PRP (QUB) are also acknowledged.

REFERENCES

- (1) Prassides, K.; Margadonna, S. In *Fullerenes: Chemistry, Physics and Technology*; Kadish, K. M., Ruoff, R. S., Eds.; John Wiley & Sons, Inc., 2000; pp 249–251, 555–610.
- (2) Dresselhaus, M. S.; Dresselhaus, G.; Eklund, P. C. *Science of Fullerenes and Carbon Nanotubes*; Academic Press, Inc., 1996; pp 184–197, 243–246.
- (3) Stephens, P. W.; Mihaly, L.; Lee, P. L.; Whetten, R. L.; Huang, S.-M.; Kaner, R.; Deiderich, F.; Holczer, K. Structure of Single-Phase Superconducting K_3C_{60} . *Nature* **1991**, *351*, 632–634.
- (4) Hebard, A. F.; Rosseinsky, M. J.; Haddon, R. C.; Murphy, D. W.; Glarum, S. H.; Palstra, T. T. M.; Ramirez, A. P.; Kortan, A. R. Superconductivity at 18 K In Potassium-Doped C_{60} . *Nature* **1991**, *350*, 600–601.
- (5) Yildirim, T.; Fischer, J. E.; Harris, A. B.; Stephens, P. W.; Liu, D.; Brard, L.; Strongin, R. M.; Smith, A. B. Orientational Phase Transition in Na_xC_{60} ($1 < x < 3$). *Phys. Rev. Lett.* **1993**, *71*, 1383–1386.
- (6) Geim, A. K.; Grigorieva, I. V. Van der Waals Heterostructures. *Nature* **2013**, *499*, 419–425.
- (7) Geim, A. K. Graphene: Status and Prospects. *Science* **2009**, *324*, 1530–1534.
- (8) Geim, A. K.; Novoselov, K. S. The Rise of Graphene. *Nat. Mater.* **2007**, *6*, 183–191.
- (9) Santos, E. J. G. Carrier-Mediated Magnetoelectric Coupling in Functionalized Graphene. *ACS Nano* **2013**, *7*, 9927–9932.
- (10) Santos, E. J. G. Magnetoelectric Effect in Functionalized Few-Layer Graphene. *Phys. Rev. B: Condens. Matter Mater. Phys.* **2013**, *87*, 15540–15547.
- (11) Li, Z. Q.; Henriksen, E. A.; Jiang, Z.; Hao, Z.; Martin, M. C.; Kim, P.; Stormer, H. L.; Basov, D. N. Dirac Charge Dynamics in Graphene by Infrared Spectroscopy. *Nat. Phys.* **2008**, *4*, 532–535.
- (12) Ojeda-Aristizabal, C.; Bao, W.; Fuhrer, M. S. Thin-Film Barristor: A Gate-Tunable Vertical Graphene-Pentacene Device. *Phys. Rev. B: Condens. Matter Mater. Phys.* **2013**, *88*, 035435.
- (13) Kim, K.; Lee, T. H.; Santos, E. J. G.; Jo, P. S.; Salleo, A.; Nishi, Y.; Bao, Z. Structural and Electrical Investigation of C_{60} -Graphene Vertical Heterostructures. *ACS Nano* **2015**, *9*, 5922–5928.
- (14) Lee, C. H.; Schiros, T.; Santos, E. J. G.; Kim, B.; Yager, K. G.; Kang, S. J.; Lee, S.; Yu, J.; Watanabe, K.; Taniguchi, T.; Hone, J.; Kaxiras, E.; Nuckolls, C.; Kim, P. Epitaxial Growth of Molecular Crystals on Van der Waals Substrates for High-Performance Organic Electronics. *Adv. Mater.* **2014**, *26*, 2812–2817.
- (15) Meyer, J. C.; Geim, A. K.; Katsnelson, M. I.; Novoselov, K. S.; Booth, T. J.; Roth, S. The Structure of Suspended Graphene Sheets. *Nature* **2007**, *446*, 60–63.
- (16) Prato, M.; Lucchini, V.; Maggini, M.; Stimpfl, E.; Scorrano, G.; Eiermann, M.; Suzuki, T.; Wudl, F. Energetic Preference in 5,6 and 6,6 Ring Junction Adducts of C_{60} : Fullerenoids and Methanofullerenes. *J. Am. Chem. Soc.* **1993**, *115*, 8479–8480.
- (17) Fagan, P.; Calabrese, J. C.; Malone, B. Metal Complexes of Buckminsterfullerene (C_{60}). *Acc. Chem. Res.* **1992**, *25*, 134–142.
- (18) Dean, C. R.; Young, A. F.; Meric, I.; Lee, C.; Wang, L.; Sorgenfrei, S.; Watanabe, K.; Taniguchi, T.; Kim, P.; Shepard, K. L.; Hone, J. Boron Nitride Substrates for High-Quality Graphene Electronics. *Nat. Nanotechnol.* **2010**, *5*, 722–726.
- (19) Zomer, P. J.; Dash, S. P.; Tombros, N.; van Wees, B. J. A Transfer Technique for High Mobility Graphene Devices on Commercially Available Hexagonal Boron Nitride. *Appl. Phys. Lett.* **2011**, *99*, 232104–232109.
- (20) Bao, W.; Liu, G.; Zhao, Z.; Zhang, H.; Yan, D.; Deshpande, A.; LeRoy, B.; Lau, C. N. Lithography-Free Fabrication of High Quality Substrate-Supported and Freestanding Graphene Devices. *Nano Res.* **2010**, *3*, 98–102.
- (21) Soler, J. M.; Artacho, E.; Gale, J. D.; Garcia, A.; Junquera, J.; Ordejon, P.; Sanchez-Portal, D. The SIESTA Method for *ab Initio* Order-N Materials Simulation. *J. Phys.: Condens. Matter* **2002**, *14*, 2745–2779.
- (22) Kresse, G.; Hafner, J. *Ab Initio* Molecular Dynamics for Open-Shell Transition Metals. *Phys. Rev. B: Condens. Matter Mater. Phys.* **1993**, *48*, 13115–13118.
- (23) Kresse, G.; Furthmüller, J. Efficient Iterative Schemes for *Ab Initio* Total-Energy Calculations Using a Plane-Wave Basis Set. *Phys. Rev. B: Condens. Matter Mater. Phys.* **1996**, *54*, 11169–11186.
- (24) Perdew, J. P.; Burke, K.; Ernzerhof, M. Generalized Gradient Approximation Made Simple. *Phys. Rev. Lett.* **1996**, *77*, 3865–3868.
- (25) Dion, M.; Rydberg, H.; Schroder, E.; Langreth, D. C.; Lundqvist, B. I. Van der Waals Density Functional for General Geometries. *Phys. Rev. Lett.* **2004**, *92*, 246401–246405.
- (26) Bautista-Flores, C.; Sato-Berrú, R. Y.; Mendoza, D. Charge Transfer in the Fullerene C_{60} -Few Layer Graphene System and the Existence of Negative Photoconductivity. *Appl. Phys. Lett.* **2014**, *105*, 191116.
- (27) Inawali, G.; Rao, Y.; Beck, J. H.; Petrone, N.; Kymissis, I.; Hone, J.; Heinz, T. F. Observation of Ground- and Excited-State Charge Transfer at the C_{60} /Graphene Interface. *ACS Nano* **2015**, *9*, 7175–7185.
- (28) Wang, R.; Wang, S.; Wang, X.; Meyer, J. A. S.; Hedegard, P.; Laursen, B. W.; Cheng, Z.; Qiu, X. Charge Transfer and Current Fluctuations in Single Layer Graphene Transistors Modified by Self-Assembled C_{60} Adlayers. *Small* **2013**, *9*, 2420.
- (29) Chaturvedi, P.; Matte, H. S. S. R.; Voggu, R.; Govindaraj, A.; Rao, C. N. R. Self-Assembly of C_{60} SWNTs and Few-Layer Graphene and Their Binary Composites at the Organic-Aqueous Interface. *J. Colloid Interface Sci.* **2011**, *360*, 249–255.
- (30) Novoselov, K. S.; Geim, A. K.; Morozov, N.; Jiang, D.; Zhang, Y.; Dubonos, S. V.; Grigorieva, I. V.; Firsov, A. A. Electric Field Effect in Atomically Thin Carbon Films. *Science* **2004**, *306*, 666–669.